Chinese Journal of Catalysis 38 (2017) 636–650

available at www.sciencedirect.com

ScienceDirect

journal homepage: www.elsevier.com/locate/chnjc

Article

Supercritical synthesis of platinum-modified titanium dioxide for solar fuel production from carbon dioxide

Susana Tostón, Rafael Camarillo *, Fabiola Martínez, Carlos Jiménez, Jesusa Rincón

University of Castilla-La Mancha, Department of Chemical Engineering, Faculty of Environmental Sciences and Biochemistry, Avda. Carlos III, s/n, 45071 Toledo, Spain

ARTICLE INFO

Article history:
Received 21 November 2016
Accepted 21 December 2016
Published 5 April 2017

Keywords:
Titanium dioxide
Platinum
Photocatalyst
Metal dispersion
Carbon dioxide photoreduction

ABSTRACT

This paper investigates the properties of TiO_2-based photocatalysts synthesised under supercritical conditions. Specifically, the characteristics of Pt dispersed on TiO_2 catalysts obtained in supercritical CO_2 are discussed and compared with those of commercial TiO_2. The photocatalytic activity of the synthesised catalysts in the CO_2 photoreduction reaction to produce solar fuel is tested. The main conclusion of the study is that photocatalysts with better or similar features, including high surface area, crystallisation degree, hydroxyl surface concentration, pore volume, absorbance in the visible range and methane production rate, to those of commercial TiO_2 may be produced for the reduction of CO_2 to fuel by synthesis in supercritical media.

© 2017, Dalian Institute of Chemical Physics, Chinese Academy of Sciences.
Published by Elsevier B.V. All rights reserved.

1. Introduction

The increasing atmospheric concentration of greenhouse gases, especially CO_2, is a pressing social issue at present [1]. Different processes to capture gas from large point sources such as the flue gases of coal, oil, natural gas and biomass power plants have been patented in recent years [2,3]. The recovered CO_2 can be either stored in natural caves or used as feedstock to produce useful chemicals, especially fuel, which is the only CO_2 conversion product that may substantially lower anthropogenic CO_2 emissions because of its high rate of consumption. However, because the CO_2 molecule is very stable, only a few technologies for its conversion are available. In particular, effective photocatalytic conversion of CO_2 to fuel has been demonstrated [4,5]. Thus, following this previous work, the present study focuses on the synthesis of catalysts for the photocatalytic conversion of CO_2 gas into fuel using solar energy (i.e., catalysts for solar fuel production from CO_2), a process with an enormous future potential despite being in the early stages of development.

The main drawbacks currently limiting photocatalytic CO_2 reduction are low photoconversion speed and efficiency. These problems may be overcome through the design of highly active photocatalysts with favourable reactant adsorption, charge separation and transport, light harvesting and CO_2 activation [6–14]. TiO_2 particles show most of these features along with non-toxicity, high photostability, chemical inertness, environmentally friendly nature and low cost. Thus, TiO_2 is a promising material for use as a catalyst in CO_2 photoreduction.

The main weakness of TiO_2 is that it only uses the ultraviolet (UV) region of the solar spectrum, which is less than 5% of the total solar energy. Moreover, after UV irradiation of TiO_2 with an energy equal or larger than its band gap (3.2 eV), the resulting photogenerated electron–hole pairs rapidly recombine.

* Corresponding author. E-mail: rafael.camarillo@uclm.es
This work was supported by Spanish Government (Project CTM 2011-26564), Regional Government of Castilla-La Mancha (Project PEII10-0310-5840), and Iberdrola Foundation (Research Grant in Energy and the Environment 2010/12 for Susana Tostón).
DOI: 10.1016/S1872-2067(17)62766-9 | http://www.sciencedirect.com/science/journal/18722067 | Chin. J. Catal., Vol. 38, No. 4, April 2017

However, both problems can be tackled with appropriate dispersion or doping of TiO_2 with either noble or transition metals [7,9,10,12,15–17]. The dispersion method leads to the scattering of metal particles on the TiO_2 support, while doping involves the inclusion or substitution of foreign metal atoms into the TiO_2 lattice [10,18].

The most commonly ascribed effect of Pt as a dopant for TiO_2 is its ability to promote charge carrier separation because electrons tend to accumulate on the doped Pt and holes remain on TiO_2. Pt also shifts the band edges of TiO_2 to make certain electron transfer processes more favourable in the vicinity of the metal atom. In addition, Pt increases the electron scavenging capability of O_2, removes strongly bound intermediates, promotes hydroxyl (OH) formation and promotes H^+ reduction to adsorbed H atoms [18]. However, the influence of Pt on TiO_2 photocatalysis is not always positive because Pt atoms may act as charge recombination centres or block active sites on TiO_2. Moreover, Pt is a good centre for hydrogen (H_2) generation from H_2O; therefore, it is necessary to take measures to minimise this process [19].

The amount of Pt added to TiO_2 can also play a major role in catalyst performance. The typical optimal Pt loading is around 1 wt% [9,18]. Higher metal contents can induce faster electron–hole recombination and deactivate the photocatalyst [10,20]. Table 1 summarises details of some recent Pt/TiO_2 catalysts. Pt concentration is typically in the range of 0.2–5 wt%.

Many studies have focused on how metal dispersion methods affect the photocatalytic behaviour of catalysts [10,18]. Several techniques have been used to disperse Pt atoms on TiO_2 substrates [21–25,27]. One method is co-precipitation in supercritical fluids because if a metal precursor is added to a reaction medium together with a Ti precursor and a hydrolysis agent, a metal dispersed on TiO_2 catalyst can be obtained in situ [28]. The use of supercritical fluids, mainly CO_2 and H_2O, for particle generation and precipitation is attractive because of their excellent properties [29,30]—they can diffuse through solids like a gas and dissolve materials like a liquid—and their ability to be adjusted by simply changing the operating parameters [31,32]. Both the fluid properties and easy tuning of supercritical fluids allow particle characteristics such as structure, morphology, size and size distribution to be controlled. All of these characteristics are very important for the final application of a catalyst [28]. Moreover, synthesis using supercritical fluids is more environmentally sustainable than classical synthesis procedures, which usually use large amounts of organic solvents.

The objective of this investigation is to use a supercritical medium to synthesise a TiO_2-based catalyst with superior performance to that of a commercial semiconductor in the photocatalytic reduction of CO_2 to fuel molecules. Specifically, Pt dispersed on TiO_2 is synthesised by a hydrothermal method using supercritical CO_2. Pt(II) acetylacetonate and titanium tetraisopropoxide (TTIP) or diisopropoxy titanium bis(acetylacetonate) (DIPBAT) are used as chemical precursors of Pt and TiO_2, respectively, with isopropyl alcohol or ethanol as a hydrolytic agent. The synthesis involves the following process. Once the reagents are in the supercritical phase, precursor decomposition occurs and alcohol decomposition provides the necessary H_2O for the hydrolysis reaction [33,34]. The end products are Pt dispersed on TiO_2 solid particles and carbonaceous contaminants originating from the precursors. The decompressed solvent is in gas phase, which facilitates catalyst drying and recovery at the end of the process. To remove carbon (C) contaminants from the catalyst, a calcination step is performed after supercritical synthesis [35].

The properties of the Pt/TiO_2 catalysts are determined by usual characterisation methods, including scanning electron microscopy (SEM), transmission electron microscopy (TEM), X-ray photoelectron spectroscopy (XPS), atomic emission spectroscopy with inductively coupled plasma (ICP-AES), X-ray diffraction (XRD), N_2 adsorption-desorption measurements, diffuse-reflectance UV-visible (DRUV-vis) spectroscopy, Fourier transform infrared (FTIR) spectroscopy and laser diffraction, and compared with those of commercial TiO_2. Their photocatalytic activity in CO_2 photoreduction to produce solar fuel is also tested.

2. Experimental

2.1. Chemicals

Various samples of Pt dispersed on TiO_2 powder were synthesised by thermal hydrolysis of two different precursors (DIPBAT and TTIP) with two different alcohols in the presence of Pt(II) acetylacetonate using supercritical CO_2 as the reaction medium. DIPBAT (75 wt% in isopropyl alcohol), TTIP (pure) and Pt(II) acetylacetonate (97 wt%) were provided by Sigma-Aldrich. Analytical reagent-grade ethanol and isopropyl alcohol were provided by Scharlab. In all analyses, Degussa

Table 1
Overview of Pt/TiO_2-based catalysts.

Support	Pt concentration (wt%)	Method	Ref.
TiO_2 anatase	0.5–2	Impregnation + air drying + calcination (450 °C, 4 h) + H_2 reduction	[21]
TiO_2 anatase	5	Mixture of TiO_2 precursor and dopant solutions + drying + gel grinding + calcination (500 °C, 5 h)	[22]
Mesoporous TiO_2 thin films	0.5–3	Evaporation induced self-assembly	[23]
TiO_2	0.2–1	Sol-gel	[24]
TiO_2	0.15	Sol-gel	[25]
TiO_2	1	Two step hydrothermal route	[20]
TiO_2	0.1–0.4	Sol-gel	[26]

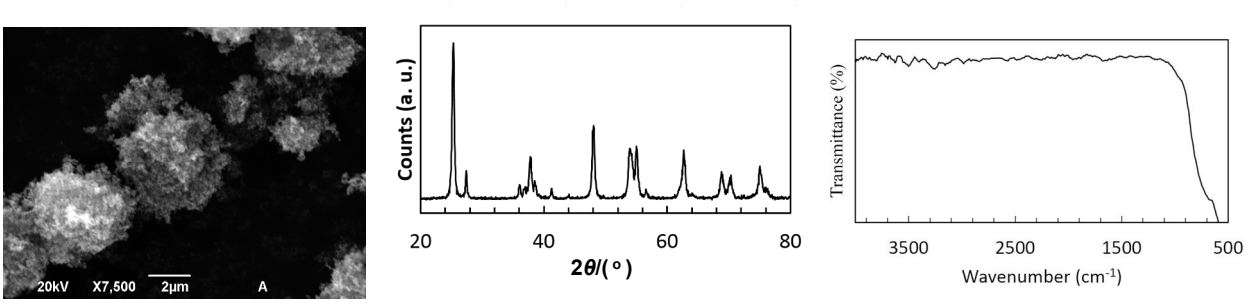

Fig. 1. SEM image (left), XRD pattern (middle) and FTIR spectrum (right) of commercial P-25 catalyst.

P-25 (Evonik) TiO_2 powder was used as a reference. Some characteristics of this commercial catalyst are shown in Fig. 1 for comparison with those of the catalysts synthesised in this work. Supercritical CO_2 (purity >99.9%, Carburos Metálicos S.A.) was used as received.

2.2. Synthesis of catalysts

The experimental set-up depicted schematically in Fig. 2 was used to synthesise photocatalysts in supercritical CO_2 in discontinuous mode. The set-up consisted of a high pressure pump (Thar SFC, P-series) preceded by a thermostated bath (Selecta, Frigiterm-30) and followed by a high pressure synthesis reactor (DEMEDE Engineering & Research, 100 mL). To synthesise the catalysts, the alcohol and Ti and Pt precursors were first added to the reactor. The system was sealed and then CO_2 was pumped into the reactor after being cooled in the thermostated bath. The high pressure pump and an electric resistor were used to reach and maintain the operating pressure and temperature in the reactor. After synthesis, the system was depressurised by opening valve V3 and the catalyst was collected from the reactor. Further details of this procedure are given elsewhere [34].

Catalyst synthesis was conducted at a pressure of 20 ± 0.2 MPa and temperature of 300 ± 5 °C using a molar ratio of 28 mmol alcohol/mmol precursor except for in the case of the ethanol/DIPBAT combination of reactants. Given that DIPBAT is a solution in isopropyl alcohol, the molar ratio used in this case was 28 mmol ethanol/mmol DIPBAT, although the test was actually performed in an alcohol mixture [33]. An appropriate amount of Pt(II) acetylacetonate was added to give final

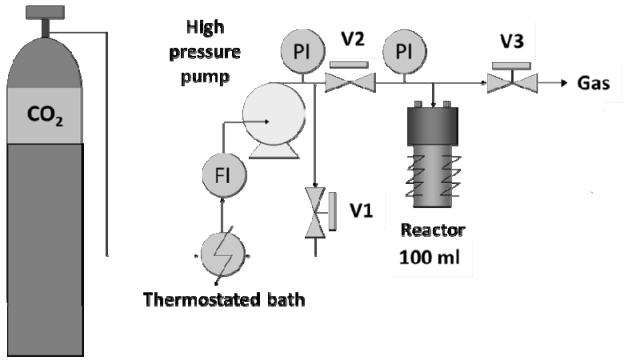

Fig. 2. Experimental system used to synthesise TiO_2-based catalysts.

Pt concentrations in the range of 1–3 wt%. Catalyst synthesis was performed for 2 h once the experimental conditions were reached. All syntheses were repeated three times. After the synthesised catalysts were removed from the reactor, they were dried at 105 °C for 12 h and then calcined at 400 °C for 6 h to remove any C contaminants from the catalysts [35].

2.3. Catalyst characterisation

The TiO_2-based catalysts were characterised by different techniques. The real percentage of Pt was measured by ICP-AES (Varian, Liberty Sequential). The detection limit of the ICP spectrometer was 20 ppb Pt. The particle size and external morphology of the particles were observed by SEM using a scanning electron microscope (JEOL, 6490 LV). TEM and high-resolution TEM were measured with a JEOL 2100 TEM operating at 200 kV equipped with a side-entry double-tilt (± 25°) sample holder and energy-dispersive spectroscopy detector (Oxford Link). XPS was conducted using an ultra-high-vacuum Specs Phoibos-150 electron spectrometer. The spectra were obtained with a photon energy of 1486.6 eV (Al anode). All binding energies were referenced to the C 1*s* peak originating from surface adventitious C at 284.6 eV. The crystallinity and crystalline phase of the catalysts were determined by powder XRD using an X-ray diffractometer (Philips, X´Pert MPD). The crystallite sizes of the TiO_2 photocatalysts were estimated *via* the Scherrer equation using the peak at $2\theta = 25.4°$. The specific surface area of the powders was evaluated using a Brunauer-Emmett-Teller (BET) area analyser (Micromeritics, ASAP 2020). DRUV-vis spectra of all catalysts were obtained on a DRUV-vis spectrophotometer (JASCO, V650). Absorbance thresholds and band gap energies (*E*g) were calculated from these spectra. FTIR spectra of all samples were obtained with a FTIR attenuated total reflectance spectrometer (Thermo Nicolet, Avatar 370 FT-IR). Particle size and particle size distribution were calculated using a laser scattering particle size distribution analyser (Malvern, Mastersizer 2000).

2.4. Photocatalytic reaction tests

The photocatalytic activities of the catalysts in photocatalytic CO_2 reduction experiments were assessed using an experimental set-up consisting of a stainless steel chamber (50 cm^3) (Fig. 3) with valves for evacuation, gas introduction and connection to a gas chromatography (GC) system, an

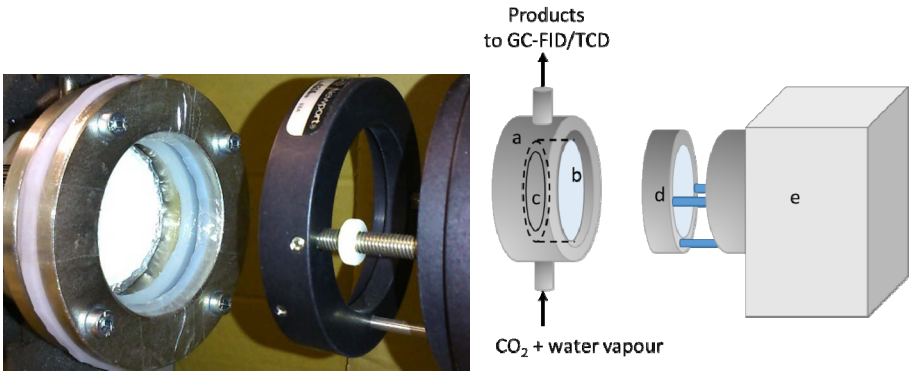

Fig. 3. Details of the photocatalytic reactor. (a) 50-cm³ stainless steel chamber; (b) O-ring-sealed quartz window; (c) filter with catalyst sample; (d) Air Mass 1.5 Global filter; (e) Xe arc lamp.

O-ring-sealed quartz window at the top to admit radiation from a Xe arc lamp (Oriel, 450 W) with an Air Mass 1.5 Global filter and a dew point transmitter and different manometers to measure relative humidity and pressure, respectively, during the reaction. A bubbler containing deionised H_2O was positioned before the reaction chamber. The beam of the lamp was diverged with a collimator with the aim of having the inside of the reaction chamber at the same irradiance as that of the sun (100 mW/cm²) to simulate solar radiation. It is possible that this irradiance decreased slightly with the use of the lamp, but this should have been negligible according to the manufacturer. Additional information can be found in a previous study [34].

Most experiments described in this paper were performed with a H_2O vapour/CO_2 ratio of 2:7, although other ratios were also assessed (2:20 and 2:1). The H_2O vapour/CO_2 ratio was increased by using the same amount of H_2O vapour and decreasing the amount of CO_2. However, to operate the photoreactor at constant pressure, appropriate quantities of an inert gas (He) were fed into the system. We operated the system in this way because if we tried to increase the H_2O vapour/CO_2 ratio by increasing the partial pressure of H_2O vapour while keeping the CO_2 amount constant, the H_2O vapour saturation pressure was reached and H_2O condensed. Other variables like catalyst weight (34.6–75.5 mg) and reaction time (3–4 h) were also evaluated. The initial absolute pressure in the reactor was 1.07 bar in all experiments.

To quantitatively and qualitatively measure the different species in the reaction chamber, a GC analytical method was developed. The gas chromatograph (Agilent GC 7890A) possessed two thermal conductivity (TCD) detectors and a flame ionisation detector (FID) with a methaniser, which made it possible to determine gases such as CO, CO_2, CH_4, light hydrocarbons (C1–C7), light alcohols, ethers and ketones. H_2 could not be analysed in the system because of technical limitations. Specifically, because He was used to increase the H_2O vapour/CO_2 ratio in the photocatalytic reactor, H_2 and He were both present in the gas stream leaving the photoreactor. These gases could not be quantified separately because the signals for both He and H_2 were detected in the same channel and with similar retention times. Nevertheless, according to the literature [36], in all the experiments performed in this work, the H_2 produced should be negligible.

In previous experiments with Degussa-P25 conducted at a higher H_2O/CO_2 ratio (2 g H_2O/g CO_2) than in the present work, CH_4, CO and H_2 production rates were 0.025, 1.233 and 0.005 μmol g^{-1} h^{-1}, respectively. Therefore, the amount of H_2 generated during the experiments described in the present work should be less than 0.005 μmol g^{-1} h^{-1}.

3. Results and discussion

3.1. Synthesis yield

The yield is the ratio between the moles of catalyst produced during synthesis with supercritical CO_2 and the moles of precursor used, taking into account that the synthesis reaction involves a 1:1 ratio for both precursors (1 mol precursor : 1 mol product). The yields obtained are presented in Table 2. Reported yields are the average of triplicate experiments. The two highest yields (85.5% and 72.0%) were achieved when TTIP was used. Furthermore, the average yield attained in the six experiments performed with TTIP was higher than the average yield of the six runs carried out with DIPBAT (66.5% with TTIP *vs.* 62.4% with DIPBAT). In principle, these results could be attributed to the higher thermal and kinetic stability of DIPBAT compared with that of TTIP. TTIP is easily hydrolysable, even at ambient temperature, in the presence of humidity because it has four isopropoxy ligands coordinated to its Ti

Table 2
Synthesis yields of different catalysts.

Combination	Precursor (mmol)	TiO_2 (mmol)	Yield (%)
TTIP-isopropyl alcohol-1%Pt	4.889 ± 0.003	2.8 ± 0.4	57 ± 8
TTIP-isopropyl alcohol-2%Pt	4.889 ± 0.003	3.1 ± 0.4	63 ± 8
TTIP-isopropyl alcohol-3%Pt	4.889 ± 0.003	3.2 ± 0.4	66 ± 8
TTIP-ethanol-1%Pt	4.889 ± 0.003	4.2 ± 0.4	86 ± 8
TTIP-ethanol-2%Pt	4.889 ± 0.003	2.7 ± 0.4	55 ± 8
TTIP-ethanol-3%Pt	4.889 ± 0.003	3.5 ± 0.4	72 ± 8
DIPBAT-isopropyl alcohol-1%Pt	5.078 ± 0.002	2.9 ± 0.4	57 ± 8
DIPBAT-isopropyl alcohol-2%Pt	5.078 ± 0.002	3.0 ± 0.4	59 ± 8
DIPBAT-isopropyl alcohol-3%Pt	5.078 ± 0.002	3.3 ± 0.4	65 ± 8
DIPBAT-ethanol-1%Pt	5.078 ± 0.002	3.1 ± 0.4	61 ± 8
DIPBAT-ethanol-2%Pt	5.078 ± 0.002	3.4 ± 0.4	67 ± 8
DIPBAT-ethanol-3%Pt	5.078 ± 0.002	3.5 ± 0.4	69 ± 8

centre [33]. DIPBAT has two of these groups substituted by two acetylacetonate ligands, which are more thermally and kinetically stable than isopropoxy ligands. Thus, hydrolysis of DIPBAT is more difficult than that of TTIP but it allows better reaction control.

In contrast, synthesis experiments with ethanol as a hydrolytic agent gave slightly higher yields than those with isopropyl alcohol (71.2% vs. 61.8% when TTIP was used as the precursor and 64.7% vs. 60.1% in the case of DIPBAT). This is probably caused by the higher polarity of ethanol than isopropyl alcohol. Alonso et al. [33] also reported that isopropyl alcohol led to a higher degree of C contamination in catalysts, as by-product elimination deteriorated because of their lower solubility in the less polar alcohol. For this reason, all the catalysts (even the reference commercial one) were calcined at 400 °C for 6 h before conducting photocatalytic experiments. The calcination temperature was limited by the transition between anatase and rutile phases, which takes place at about 700 °C [37]. This calcination step will have important consequences for the properties of the catalysts discussed below. Regarding the effect of metal loading on yields, it can be seen that this variable does not have a clear influence on the results.

3.2. SEM, TEM, XPS and ICP-AES analyses

The morphology of the synthesised Pt/TiO_2 particles after calcination is shown in Fig. 4. Spherical particles were obtained when DIPBAT was used as a precursor. The SEM images reveal these particles were well-defined spheres with diameters of about 4–5 μm. These spherical particles are slightly bigger than those of commercial TiO_2 (Fig. 1) and reported by Alonso et al. [33], who obtained particles with diameters of 270 ± 125 nm using TTIP and 200 ± 100 nm using DIPBAT under synthesis conditions similar to those in this work (20 MPa and 300 °C). Because particle size depends on reaction temperature, the larger particles obtained here could be caused by temperature fluctuation in the reactor (300 ± 5 °C); i.e., higher temperatures (305 °C) led to larger particles. In the case of TTIP, larger polyhedral-like particles were obtained than when using DIPBAT, especially when ethanol was used as the hydrolysis agent. Some agglomeration was observed as the Pt loading increased, especially when ethanol was used as the hydrolysis agent. However, this phenomenon was largely avoided by calcination of the synthesised catalysts. It should also be highlighted that the particle sizes and shapes are similar to those obtained by other groups using supercritical fluid synthesis [33,38] and classical methods like chemical vapour deposition [39].

Regarding the effect of particle size and morphology on catalyst performance, a previous study [40] showed that photocatalytic activity tended to decrease with increasing particle size because specific surface area was lowered. Likewise, it has been demonstrated that anatase nanoparticles with polyhedral-like shapes are more active than those with rounded or spherical shapes [41].

Representative TEM images of TTIP-isopropyl alcohol-1%Pt and TTIP-isopropyl alcohol-3%Pt samples are provided in Fig. 5. In both cases, small Pt particles were uniformly dispersed over the crystalline TiO_2 particles. The size distribution of Pt is relatively narrow for both catalysts, with average particle diameters of 2.2 nm for the sample with 1% Pt and 3.5 nm for that with 3% Pt. This size range is consistent with that reported by Semlali et al. [23] for mesoporous Pt/TiO_2 thin films synthesised by evaporation-induced self-assembly with Pt loadings of 0.5–3 wt%.

The Pt concentration of the samples was measured by ICP-AES. In all cases, the total amount of Pt was incorporated into the final product during the synthesis of the Pt/TiO_2 catalyst within the interval assayed (1–3 wt% Pt).

With respect to XPS analyses, Fig. 6 shows the XPS survey spectrum of TTIP-ethanol-1%Pt. The sample contains Ti, O, C and Pt, with sharp photoelectron peaks appearing at binding energies of 458.4 eV (Ti 2*p*), 529.6 eV (O 1*s*), 284.6 eV (C 1*s*) and 68–78 eV (Pt 4*f*). The Ti 2*p* and O 1*s* peaks originated from TiO_2.

The estimated ratio between the Pt 4*f* and Ti 3*s* peak intensities at 61.8 eV leads to a relative Pt:Ti concentration of 0.6% on the TiO_2 surface, which is compatible with the expected stoichiometry in the final product (taking into account the error when predicting stoichiometry from XPS data).

The C peak is attributed to the residual C in the sample. The

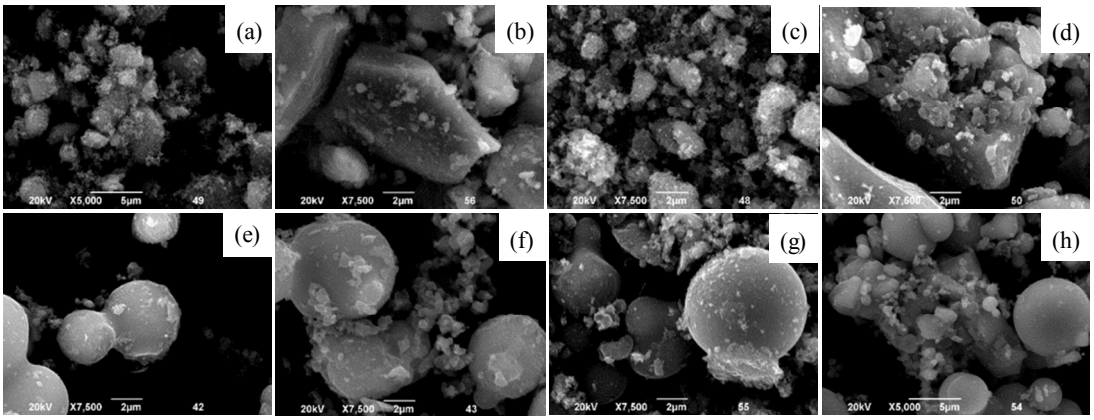

Fig. 4. SEM images of synthesised catalysts after calcination. (a) TTIP-isopropyl alcohol-1%Pt; (b) TTIP-ethanol-1%Pt; (c) TTIP-isopropyl alcohol-3%Pt; (d) TTIP-ethanol-3%Pt; (e) DIPBAT-isopropyl alcohol-1%Pt; (f) DIPBAT-ethanol-1%Pt; (g) DIPBAT-isopropyl alcohol-3%Pt; (h) DIPBAT-ethanol-3%Pt.

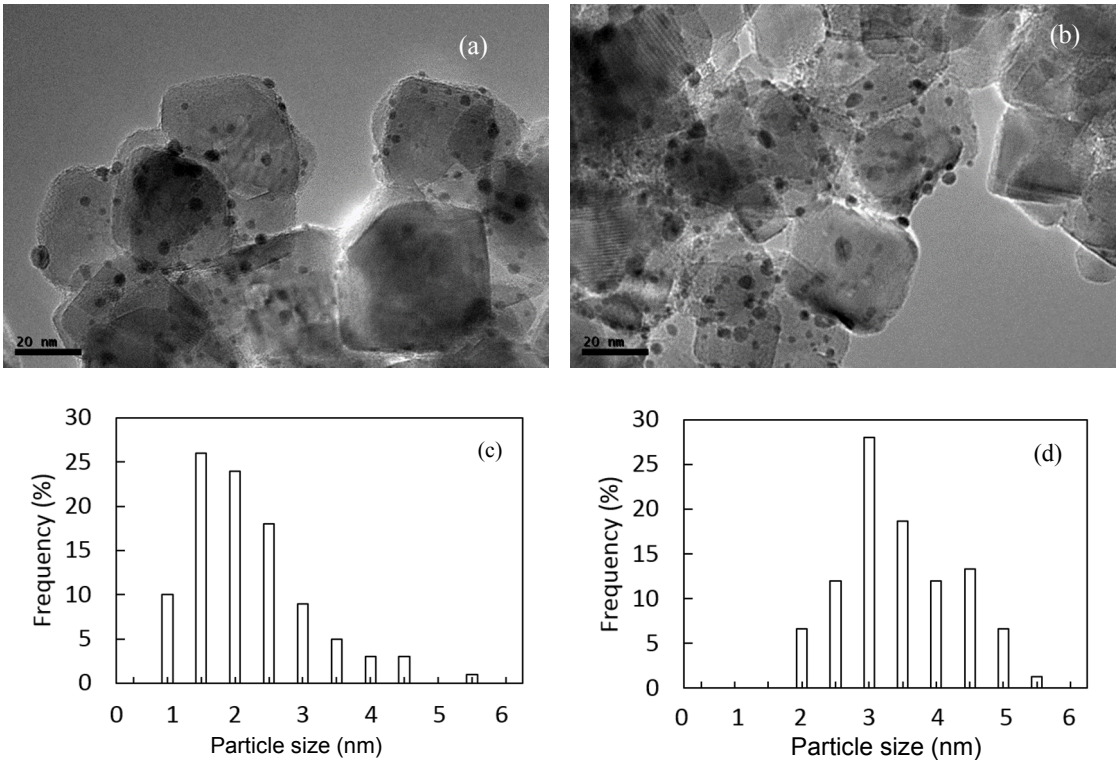

Fig. 5. Representative TEM images (a,b) and relative estimated Pt particle size distributions (c,d) of Pt/TiO_2 catalysts. (a,c) TTIP-isopropyl alcohol-1%Pt; (b,d) TTIP-isopropyl alcohol-3%Pt.

low intensity of this peak is indicative of the ready ability of the calcination process to remove precursor and alcohol C-based waste species. This peak could also arise from adventitious hydrocarbons originating from the XPS instrument itself [42].

The results of SEM, TEM, XPS and ICP-AES indicate that, from the viewpoint of morphology, the catalysts with higher photocatalytic activity will be those obtained from the TTIP-ethanol-Pt reactant combination, because they have polyhedral shapes. However, focusing on particle size, catalysts synthesised from the TTIP-isopropyl alcohol-Pt combination may also display high catalytic activity.

3.3. XRD analysis

XRD is a unique method to determine the crystallinity of a compound. Knowledge about the crystallinity of a catalyst is relevant because photocatalytic performance usually increases with crystallinity, which is usually attributed to the removal of dangling bonds and distorted lattice structure acting as recombination sites as crystallinity increases. Nevertheless, high crystallinity may also lead to decreases of surface OH coverage and total surface area and, as a consequence, poorer catalytic behaviour [18].

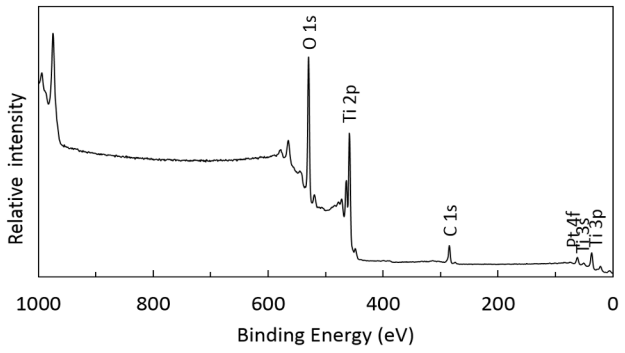

Fig. 6. XPS survey spectrum of the TTIP-ethanol-1%Pt catalyst.

XRD patterns of the catalysts obtained from the different precursor-alcohol combinations are presented in Fig. 7. The TTIP-isopropyl alcohol-Pt catalysts show the highest crystallinity (highest peak height and resolution) of the sample, very close to that of the commercial catalyst (Fig. 1). In contrast, catalysts from the other combinations exhibit poorer crystallinity, even after calcination, which usually enhances this parameter [35]. Additionally, the loading percentage of Pt does not seem to markedly affect the crystallinity of the catalysts.

Regarding crystal phase, anatase TiO_2 displays diffraction peaks at 2θ of 25.4°, 37.8°, 48.5°, 54.0°, 55.4°, 62.9°, 68.9°, 70.3° and 75.2° [43,44]. According to the patterns in Fig. 7, this allotropic phase (anatase) is the most common in the catalysts synthesised in this work. In fact, no diffraction peaks originating from any other crystal phase of TiO_2 were observed in the XRD patterns of synthesised catalysts, indicating the formation of pure anatase TiO_2. Considering the crystal phase of the catalysts before calcination, only the anatase phase was detected, as was the case in a similar study [33] with the same reagents and under the same synthesis conditions (20 MPa and 300 °C).

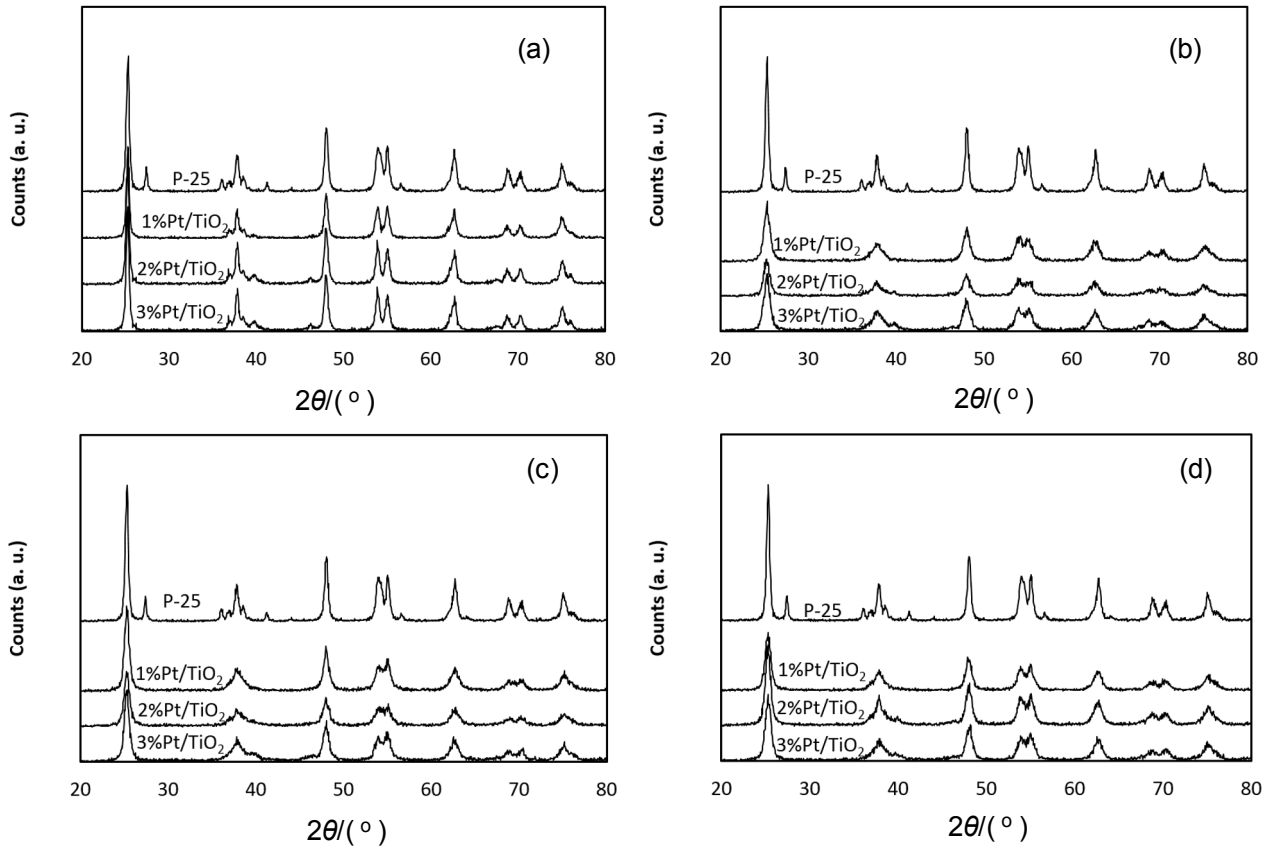

Fig. 7. XRD patterns of synthesised catalysts. (a) TTIP-isopropyl alcohol-Pt; (b) TTIP-ethanol-Pt; (c) DIPBAT-isopropyl alcohol-Pt; (d) DIPBAT-ethanol-Pt.

Metal loading does not affect the resulting crystal phase, because similar catalysts obtained in the absence of metal show only the anatase phase in their XRD patterns [45]. However, this was not the case for the commercial catalyst, because TiO_2 P-25 from Evonik (formerly Degussa) is a mixture of 80% anatase and 20% rutile phases [46]. In this case, additional peaks at 27.5°, 36.9° and 41.4° ascribed to rutile TiO_2 are observed (Fig. 1). The absence of the rutile phase in the synthesised catalysts also means that the calcination to remove all organic contaminants is conducted at an appropriate temperature that avoids phase change [47].

This result is important because anatase TiO_2 is inherently more photoactive than rutile as a result of both its solid-state properties (better light absorption and charge transport) and surface properties (larger response to charge trapping and transfer and superior chemical response to the adsorbates involved in electron transfer reactions) [18]. Fig. 7 does not contain any peaks attributable to Pt, which may be caused by the low content and high dispersity of the loaded Pt atoms [44].

Crystallite size (D) is a measure of single-crystal size, and therefore it can be interpreted as an indicator of the crystalline quality of catalyst particles. This crystal parameter has the largest effect on photocatalysis from the viewpoint of light–material interactions including photon absorption, charge-carrier generation and dynamics, and surface trapping [37]. D, which is the size of particles in the direction vertical to the corresponding lattice plane, can be determined from XRD line broadening measurements using the Scherrer equation [48]:

$$D \approx 0.9\lambda/\beta cos\theta \quad (1)$$

in this equation, λ is the X-ray wavelength (0.1541 nm), β the full width at half-maximum intensity (rad) and θ is half of the diffraction peak angle (approximately 12.7° for the <101> anatase crystal facet).

Comparison of the data in Table 3 shows that the synthesised catalysts are smaller than the commercial catalyst (19.97 nm) with the sole exception of the TTIP-isopropyl alcohol-Pt combination (D = 21.25–22.77 nm). The smallest catalyst is TTIP-ethanol-Pt (9.65–9.98 nm). All D values reported here are compatible with those found by other groups [38,49]. It should also be highlighted that, according to Table 3, the smaller particles generally have higher surface areas, although this relationship does not hold for the combination DIPBAT-ethanol-Pt. This discrepancy may be because the Scherrer equation is not completely adequate to estimate D of catalysts, despite being the most popular method for this purpose. That is, when using the Scherrer equation to calculate D from XRD data, D are assumed to be those of a coherently diffracting domain, which is not necessarily the same as particle size. The Scherrer equation attributes XRD peak broadening exclusively to crystal size, and does not take into account that crystalline defects also cause line broadening.

Table 3
Surface properties and crystallite sizes of commercial and synthesised catalysts.

Catalyst	D (nm)	S_{BET} (m^2/g)	Pore volume (cm^3/g)	Mean pore size (nm)
P-25	20	63	0.39	12.5
TTIP-isopropyl alcohol-1%Pt	23	51	0.22	9.5
TTIP-isopropyl alcohol-2%Pt	21			
TTIP-isopropyl alcohol-3%Pt	21			
TTIP-ethanol-1%Pt	10	140	0.48	7.0
TTIP-ethanol-2%Pt	10			
TTIP-ethanol-3%Pt	10			
DIPBAT-isopropyl alcohol-1%Pt	13	140	0.46	6.6
DIPBAT-isopropyl alcohol-2%Pt	11			
DIPBAT-isopropyl alcohol-3%Pt	11			
DIPBAT-ethanol-1%Pt	11	96	0.40	6.2
DIPBAT-ethanol-2%Pt	11			
DIPBAT-ethanol-3%Pt	11			

Neither the Ti precursor nor the percentage of Pt loading strongly influenced *D* when ethanol was used as the hydrolytic agent. In contrast, the catalysts synthesised with isopropyl alcohol displayed *D* that depended on the precursor; larger D was obtained with TTIP than with DIPBAT. Likewise, neither the alcohol type nor the Pt loading affected *D* when DIPBAT was used as the Ti precursor. In contrast, when TTIP was used, *D* obtained with isopropyl alcohol were larger than those with ethanol. In principle, these experimental findings should be related to the nature of the reactants (TTIP is hydrolysed more easily than DIPBAT and isopropyl alcohol is less polar than ethanol). However, we are still looking for a convincing explanation for our results.

According to the XRD analyses, TTIP-isopropyl alcohol-Pt should be the combination with the highest photocatalytic activity, because the formation of highly crystallised anatase with larger *D* might facilitate the transfer of photoelectrons, which could lower the probability of the recombination of photoinduced electrons and holes. However, as we shall see in the next section, this synthesis combination also led to small specific surface areas.

3.4. BET analysis

The specific surface area (m^2/g) is a parameter commonly used to determine the type and properties of a material regarding adsorption, heterogeneous catalysis and surface reactions. Several methods have been developed to measure the specific surface area of materials; the BET N_2 adsorption procedure is one of the most widely used. In this work, we used the BET method to determine the specific surface areas of the catalysts.

The synthesised Pt/TiO_2 catalysts displayed type-IV adsorption isotherms with one hysteresis loop at a relative pressure range of 0.5–0.8. The measured specific surface areas for the catalysts are listed in Table 3. The samples synthesised from TTIP possessed smaller average surface areas than those obtained from DIPBAT. With respect to the alcohol used in the catalyst synthesis, the results depend on the Ti precursor. The surface area results are undoubtedly related to the crystallinity of the synthesised catalysts. Thus, samples with high crystallinity, such as those synthesised from TTIP and isopropyl alcohol show smaller surface areas (Table 3). In contrast, materials with poor crystallinity (like the catalysts obtained using DIPBAT) display increased porosity and surface area. Similar findings have been reported in the literature for other nanoparticles synthesised in supercritical CO_2 [33,50]. Although it is not shown in Table 3, a slight decrease (<5%) in specific surface area with increasing Pt loading was observed for all precursor/alcohol combinations. This finding may be related to the deposition of Pt^0 nanoparticles [26].

The mean pore size in the catalysts was estimated using the Barrett-Joyner-Halenda model, while the Harkins-Jura equation was used to determine the thickness of the adsorbed N_2 layer from the adsorption data assuming cylindrical pore geometry. As shown in Table 3, all samples had mesoporous structures, which can enhance the rate of gaseous photocatalytic reactions because of the rapid diffusion of gas molecules within mesopores. According to the above results, if only surface area and pore volume are taken into account, the ideal particles for photocatalysis should be those obtained from the combinations of TTIP-ethanol-Pt and DIPBAT-isopropyl alcohol-Pt.

3.5. DRUV-vis analysis

The DRUV-vis spectra of the synthesised catalysts generally shifted toward the visible range compared with that of the reference commercial catalyst (Fig. 8). These results are of great interest because the emission spectrum of the Xe lamp used in the photocatalytic experiments to mimic the solar spectrum exhibited high irradiance in the visible range. The reason for using this lamp was to gauge the possibility of using sunlight as the energy source in future research.

Many groups have examined how loading TiO_2 with different cations shifts its absorption into the visible region [16-18]. The metal atoms act as a sink for photoexcited electrons, which enhances charge separation efficiency [51]. This increase in visible-light absorption is also associated with the formation of oxygen vacancies/Ti^{3+} species [11]. In this study, the absorbance in the visible range increased by up to ten times for TTIP-ethanol-Pt (Fig. 8(b)), DIPBAT-isopropyl alcohol-Pt (Fig. 8(c)) and DIPBAT-ethanol-Pt (Fig. 8(d)) compared with that of the commercial catalyst. In the case of TTIP-isopropyl alcohol-Pt, visible light absorption increased by seven times (Fig. 8(a)).

Regarding the effect of the Pt loading percentage in the catalyst, Fig. 8 reveals that the absorbance in the visible range is higher for the Pt/TiO_2 catalysts than for commercial TiO_2. Moreover, the absorbance intensity increased with the metal concentration for catalysts synthesized with both Ti precursors [26]. Absorption thresholds and E_g of the synthesised catalysts were calculated from the UV-vis spectra in Fig. 8, and are presented in Table 4. Each absorption threshold was obtained from the intersection of the x-axis and a line tangent to the absorption curve where the maximum slope is found [52]. A shift towards the visible region of the absorption threshold of met-

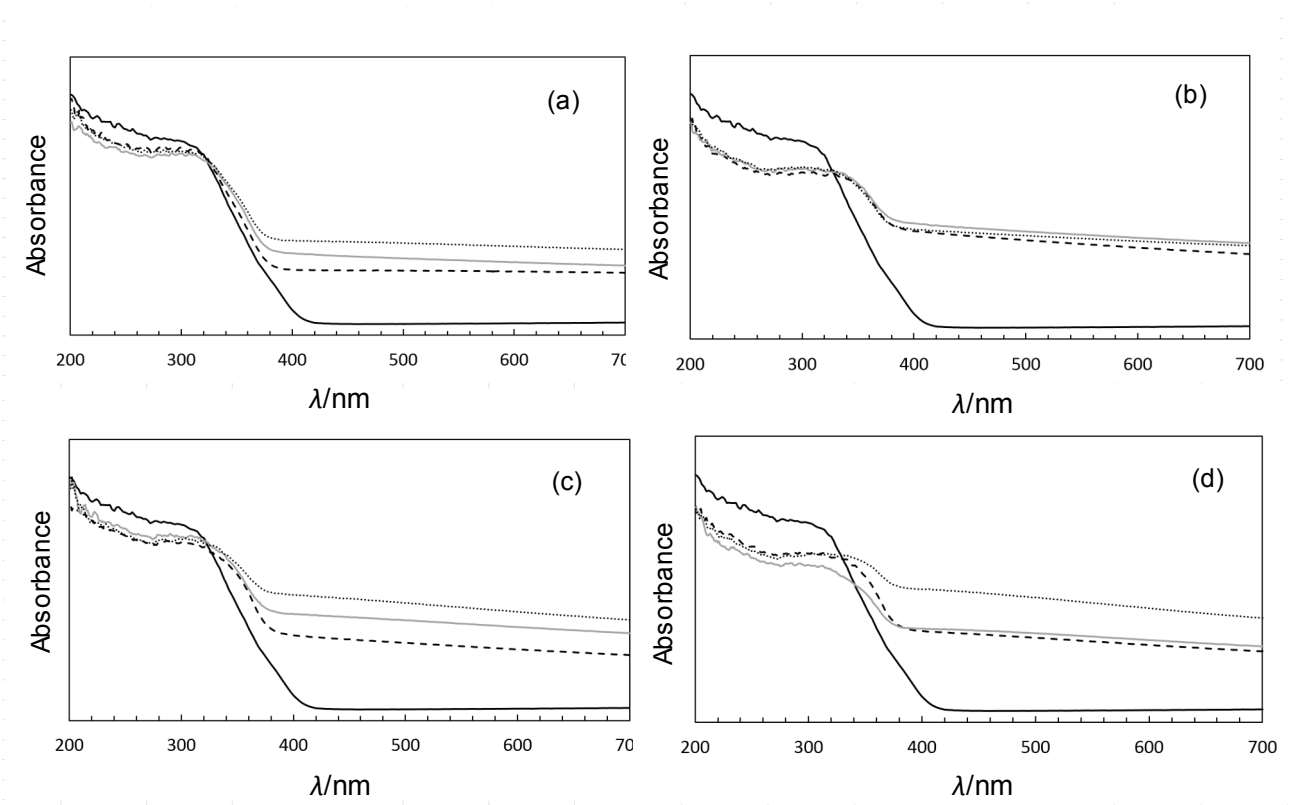

Fig. 8. DRUV-vis spectra of commercial and synthesised catalysts. (a) TTIP-isopropyl alcohol-Pt; (b) TTIP-ethanol-Pt; (c) DIPBAT-isopropyl alcohol-Pt (d) DIPBAT-ethanol-Pt (black lines: commercial, dashed lines 1% Pt, grey lines 2% Pt, dotted lines 3% Pt).

al/TiO_2 photocatalysts has been often taken as direct evidence for enhancement of their photocatalytic activity under solar or visible irradiation [52].

The band gap is the void region that extends from the top of the filled valence band to the bottom of the vacant conduction band in a semiconductor [53]. The band gap of a semiconductor catalyst defines the amount of photons that are available for quantum conversion. E_g can be calculated from equation 2, where h is the Planck constant ($4.13566733 \times 10^{-15}$ eV·s), c is the speed of light (3×10^5 km/s) and λ is absorption threshold (nm) [54].

Table 4
Absorption threshold and band gap energies of commercial and synthesised catalysts.

Catalyst	Absorption threshold (nm)	Band gap (eV)
P-25	407	3.048
TTIP-isopropyl alcohol-1%Pt	415	2.990
TTIP-isopropyl alcohol-2%Pt	427	2.906
TTIP-isopropyl alcohol-3%Pt	436	2.846
TTIP-ethanol-1%Pt	453	2.739
TTIP-ethanol-2%Pt	457	2.715
TTIP-ethanol-3%Pt	457	2.715
DIPBAT-isopropyl alcohol-1%Pt	416	2.982
DIPBAT-isopropyl alcohol-2%Pt	430	2.885
DIPBAT-isopropyl alcohol-3%Pt	471	2.834
DIPBAT-ethanol-1%Pt	426	2.812
DIPBAT-ethanol-2%Pt	447	2.776
DIPBAT-ethanol-3%Pt	483	2.669

$$E_g = \frac{h \cdot c}{\lambda} \quad (2)$$

The absorption threshold of the commercial catalyst was 407 nm, whereas those of the synthesised catalysts were higher (415–483 nm) (Table 4). The combination that gave the highest mean value was TTIP-ethanol-Pt, even though DIPBAT-ethanol-3%Pt displayed the highest individual value. The absorbance intensity in the visible range is reflected by the colour of the samples. Thus, as shown in Fig. 9, the samples with weak absorbance in the visible range (P-25) are white, those with a moderate absorbance are grey (TTIP-isopropyl alcohol-1%Pt), and those with the strongest visible absorption (TTIP-ethanol-1%Pt) are brown. It should be noted that Fig. 9 depicts the photographs of the catalysts after use in the photocatalytic reaction, although their colour was similar before reaction. Another interesting observation in Fig. 8 is that only one absorption edge can be detected in the DRUV-vis spectra, indicating that the catalysts behave as a single phase rather than a mixture of compounds with different absorption thresholds [52]. Moreover, there is a linear correlation between the absorption threshold and the amount of Pt in the catalysts.

Similarly, while E_g of the commercial catalyst was 3.048 eV (pure anatase: 3.2 eV), all the synthesised catalysts showed E_g in the range of 2.669–2.990 eV. This means that the energy required to excite the synthesised catalysts is lowered because extra levels are introduced in the gap region below the conduction band of TiO_2 [6,15]. This decrease in excitation energy

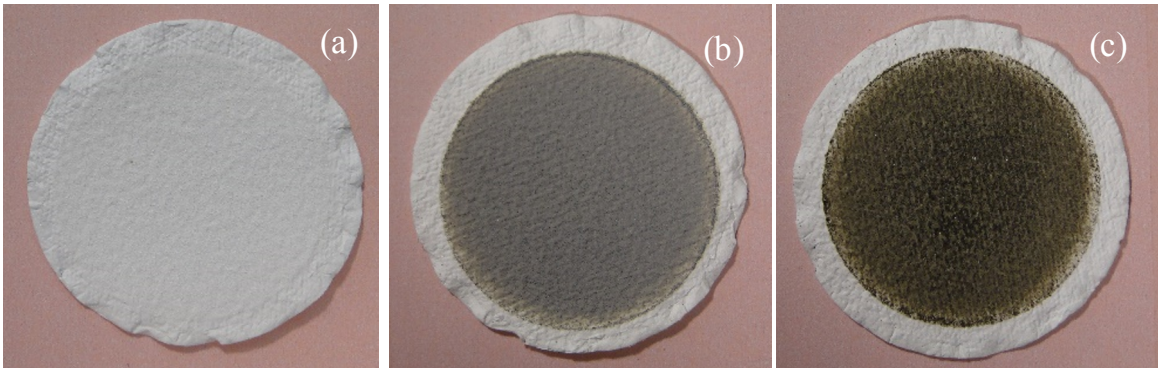

Fig. 9. Photographs of filters with catalysts after photocatalytic experiments. (a) Commercial; (b) TTIP-isopropyl alcohol-1%Pt; (c) TTIP-ethanol-1%Pt.

allows more efficient use of the visible spectrum by the Pt/TiO_2 catalysts [15,55].

Notably, the combinations with the lowest mean band gap value are TTIP-ethanol-Pt (2.723 eV) and DIPBAT-ethanol-Pt (2.752 eV). This variable decreased less than 5% as Pt loading increased from 1 to 3 wt%. For this reason, all the photocatalytic experiments were performed using catalysts with a Pt loading of 1 wt%. If these results are compared with those from catalysts synthesised in the absence of Pt [45], the adsorption threshold and E_g of every Pt/TiO_2 catalyst are higher and smaller, respectively, than those of the corresponding catalyst without Pt. Thus, the introduction of Pt has a positive influence on the light harvesting ability of TiO_2. In short, the absorbance of the synthesised catalysts is increased in the visible range compared with that of P-25, especially when ethanol is used as the hydrolysis agent.

3.6. FTIR analysis

The FTIR spectrum of the commercial P-25 catalyst (Fig. 10) only shows a peak around 690 cm^{-1}, which corresponds to Ti–O–Ti bonds [56].

The FTIR spectra of the synthesised catalysts are generally similar to that of the commercial catalyst (Figure 10). Some of the catalysts show a small peak around 1625 cm^{-1} and/or a wide band centred at 3000 cm^{-1}, which are attributed to stretching vibrations of OH groups and H_2O on the catalyst surface [57,58]. In principle, as explained above, the presence of these species usually favours the photocatalytic process [18]. The presence of OH groups (Brønsted acid sites) is beneficial for the reduction of CO_2, because they lead to efficient charge separation and transfer to the TiO_2 surface [11]. The above-mentioned peaks mainly appear in catalysts that use ethanol as the hydrolysis agent, especially the combination TTIP-ethanol-Pt. In the case of DIPBAT-ethanol-Pt, these peaks disappear when the Pt content exceeds 1 wt%.

3.7. Particle size and particle size distribution

Particle size distribution and mean particle size are two important parameters of particulate materials. Both variables have a strong influence on other previously mentioned parameters such as surface area and porosity [33,38,50], which determine the efficiency of photocatalysis because they provide a contacting surface between catalyst, light and reactants.

Regarding mean particle size, the mean size of the commercial catalyst (3 μm) is considerably smaller than those of the synthesised catalysts; for example, 8.75 μm for TTIP-ethanol-1%Pt. These results are in accordance with the SEM images of the synthesised catalysts. The particle size distributions of the synthesised catalysts are wide; only 50% of particles are around 5 μm in size, whereas the commercial catalyst has 72% of particles with sizes in the range from 0.6–5 μm.

Considering the effects of the reagents used on particle size, the influence of both precursors on particle size is smaller than those of the alcohol employed and metal loading. Thus, the introduction of ethanol and a larger amount of Pt facilitate increased particle sizes and aggregation, as indicated in SEM measurements. These results agree with those reported by Alonso et al. [33]. Decreasing particle size leads to increased surface energy, lattice distortion/strain and changed surface dangling bond population, which means that TiO_2 surface properties improve as particle size decreases [18]. In other words, if only surface properties are considered, the commercial catalyst should show higher photocatalytic activity than the synthesised catalysts.

3.8. Photocatalytic activity in CO_2 reduction

The majority of photocatalytic CO_2 reduction studies have been performed in liquid media using H_2O as the solvent. However, one important issue when studying this process is the physical state in which it is carried out. For example, although CO_2 photoreduction in liquid H_2O is relatively simple, certain problems arise because of both the low solubility of CO_2 in H_2O and the existence of competing reactions that consume holes and electrons, leading to the formation of H_2 and H_2O_2 at the expense of CO_2 reduction products (methanol, CH_4, CO, *etc.*) [59]. Furthermore, if CO_2 reduction is performed in liquid H_2O, CO_2 is in the form of carbonates or bicarbonates, which are more difficult to reduce than CO_2 itself [6]. Thus, it has been

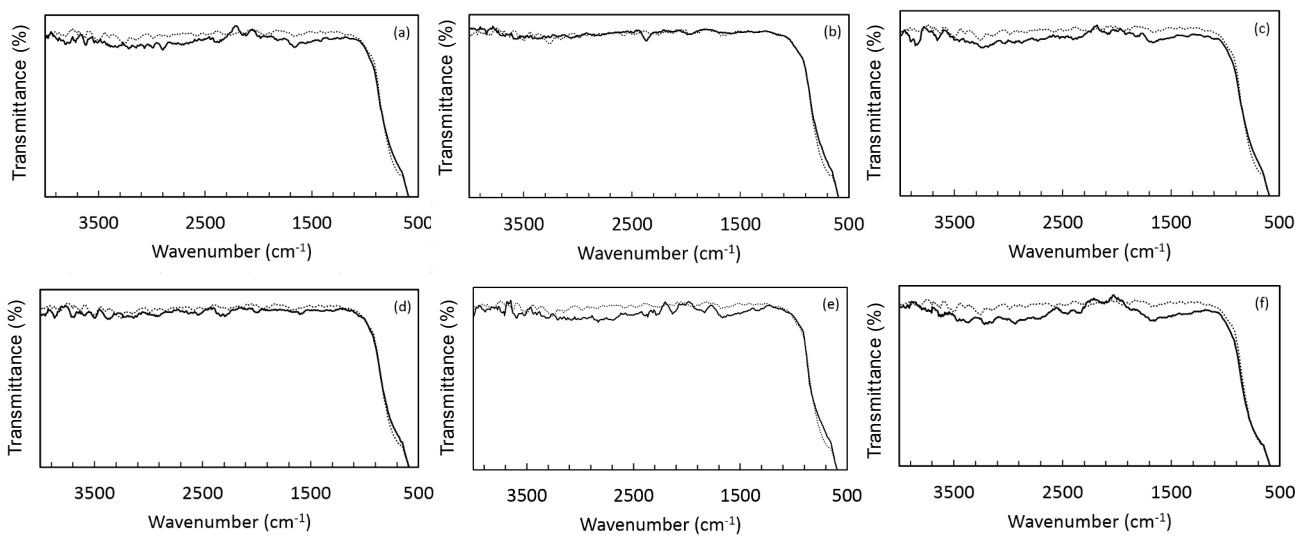

Fig. 10. FTIR spectra of synthesised catalysts (solid lines) and P-25 (dotted lines). (a) TTIP-ethanol-1%Pt; (b) TTIP-isopropyl alcohol-1%Pt; (c) TTIP-ethanol-2%Pt; (d) DIPBAT-isopropyl alcohol-1%Pt; (e) TTIP-ethanol-3%Pt; (f) DIPBAT-ethanol-1%Pt.

found that when liquid H_2O is used as the reaction medium, organic yields are low [59]. To avoid such liquid-phase reaction problems, some authors have proposed working under gas-phase conditions [35,55]. Moreover, this would provide an additional advantage because in the reactions with H_2O vapour, the photocatalyst is immobilised, which simplifies the separation of products from the catalyst. For all these reasons, we decided to test the activity of the synthesised catalysts by performing CO_2 photoreduction in the gas phase. Different series of blank experiments ((a): in the absence of photocatalyst, (b): in the dark and (c): only with wet He (in the absence of CO_2)) were performed, after which no reaction product containing C was detected, except for CO_2 in series (a) and (b) (data not shown). Table 5 presents the results obtained with commercial and synthesised catalysts in the presence of light and CO_2.

Table 5 reveals that the main reaction products were CH_4 and CO, a result consistent with one of the popular possible reduction mechanisms described in the literature [49] and with experimental results from other authors. For example, Yui et al. [60] reported that the main product from CO_2 photoconversion was CO and that substantial quantities of CH_4 were obtained only after introducing a metal onto TiO_2. Mao et al. [44] later confirmed this finding, reporting that CH_4 was the main conversion product of CO_2 photoreduction using Pt dispersed on TiO_2 as a catalyst.

Four preliminary tests were carried out with commercial P-25 as the catalyst to select the operating conditions (amount of catalyst and H_2O vapour/CO_2 ratio) for the photocatalytic experiments with synthesised Pt dispersed on TiO_2 catalysts (Table 5). These tests were also intended to gather data to compare the performance of commercial TiO_2 and Pt/TiO_2 catalysts. The parameter used to assess catalyst performance was the rate of product formation. For CO_2 photoreduction, this parameter is generally expressed as the amount of product (μmol) divided by the time it took to accumulate (h) and the amount of catalyst used (g) [49]. In the assays with commercial TiO_2, Table 5 shows that the CH_4 and CO production rates were 0.033–0.078 and 1.497–2.014 μmol g^{-1} h^{-1}, respectively. The activity of P-25 may be attributed to the complementary effects of anatase and rutile phases, in which the interfaces between the phases could play a major role in catalysis [49].

The effect of H_2O vapour/CO_2 ratio on photocatalyst activity was investigated using about 35 g of TiO_2 and H_2O vapour/CO_2 ratios of 2:1, 2:7 and 2:20. Table 5 reveals that the highest total

Table 5
Results for photocatalytic reduction of CO_2.

Catalyst	Pt loading (wt%)	Catalyst weight (mg)	H_2O/CO_2 (mol/mol)	Reaction time (h)	Production rates (μmol g^{-1} h^{-1}) CH_4 (CO)
P-25	0	35.6	2/1	3	0.033 (1.497)
P-25	0	35.5	2/7	3	0.075 (2.014)
P-25	0	35.2	2/20	3	0.078 (1.875)
P-25	0	75.5	2/7	3	0.033 (1.887)
TTIP-isopropyl alcohol	1	34.6	2/7	3	0.135 (0.109)
TTIP-ethanol	1	39.6	2/7	3	0.245 (0.058)
DIPBAT-isopropyl alcohol	1	35.7	2/7	3	0.164 (0.132)
DIPBAT-isopropyl alcohol	1	36.9	2/7	4	0.172 (0.096)
DIPBAT-ethanol	1	39.3	2/7	3	0.140 (0.167)
DIPBAT-ethanol	1	37.1	2/7	4	0.131 (0.069)

Light source: Xe arc lamp (450 W).

rates (0.075 μmol CH_4 g^{-1} h^{-1} and 2.014 μmol CO g^{-1} h^{-1}) were obtained at the intermediate ratio (2:7). This result agrees with those reported in the literature because, although it is commonly believed that CO_2 reactivity increases as the proportion of H_2O is raised, it has also been reported that excess H_2O could inhibit the reaction [61]. The optimum H_2O/CO_2 ratio obtained in this work (2:7) is considerably lower than that reported by Anpo *et al*. [61] for CO_2 photoconversion in liquid H_2O (5:1). This result is very interesting because it indicates that the reaction products are far less dilute when the photoreduction process is performed in the gas phase (i.e., using H_2O vapour instead of liquid H_2O).

Considering the effect of catalyst weight, the experiments performed at a H_2O/CO_2 ratio of 2:7 with a greater weight of catalyst (75.5 g vs. 35.5 g) did not necessarily lead to the best photocatalytic performance. This may be explained by considering the well-known fact that formation rate increases linearly with catalyst concentration only up to a certain value at which decreased light penetration and increased scattering occur, limiting formation rate [49].

Regarding the effect of Pt on TiO_2 photocatalytic performance, for the experiments carried out with catalyst weights of 35–40 mg, a H_2O vapour/CO_2 ratio of 2:7 and operating times of 3–4 h, the CH_4 production rates were about 3.2 times higher using the Pt/TiO_2 catalysts than the commercial catalyst. The highest performance was obtained for the combination TTIP-ethanol-1%Pt when the operating time was 3 h. It should be noted that this catalyst had already shown superior characteristics, as illustrated in Table 6, which orders the catalysts used in the photocatalytic experiments from best to worst according to the value of the property analysed. In particular, Table 6 reveals that the characteristics that make this catalyst better than the others are its morphology (polyhedral), narrow E_g, the presence of surface OH groups, high surface area and relatively large mean pore size.

Regarding the influence of these properties of catalysts on the CO_2 photocatalysis, it should be noted that the higher the surface area is, the greater the number of reactant molecules adsorbed and the more quickly the electrons can reach them. This results in a lower recombination probability and higher product yield [10,18]. In addition, the presence of basic species (OH groups) on the catalyst surface leads to stronger interactions with CO_2 and higher uptake of this gas [10,11,18], so the larger the surface area is, the higher the catalyst activity will be.

Table 6
Ordering of catalysts used in photocatalytic tests.

Catalyst property	Desired value	Ordering of catalysts
Photocatalytic activity	High	A>B>C>D
Particle size	Small	D>A>B>C
Morphology	Polyhedral	A>D>C>B
Crystallinity	High	D>B>A>C
Band gap energy	Low	A>C>B>D
Presence of surface OH groups	High	A>C>B>D
Surface area	High	A>B>C>D
Mean pore size	High	D>A>B>C

A: TTIP-ethanol-1%Pt; B: DIPBAT-isopropyl alcohol-1%Pt; C: DIPBAT -ethanol-1%Pt; D: TTIP-isopropyl alcohol-1%Pt.

Regarding mean pore size, although small pores result in a large surface area, mesopores (as in our case: 7–10 nm) are always preferable to allow diffusion of reactant and product molecules [18]. A narrow E_g is also desired because it improves light absorption and charge carrier generation [7–10,62]. Finally, polyhedral particle shapes show higher activity than rounded particles because of their higher density of catalytically active sites, although this has not yet been fully explained [41].

The catalyst showing the second highest CH_4 production rate was DIPBAT-isopropyl alcohol-1%Pt, which also exhibited high surface area. Alonso and colleagues also obtained good results with this catalyst in the oxidation of methyl orange in aqueous solutions [38]. According to our results, surface area seems to be the most influential property on the catalyst activity in reduction of CO_2 to fuel molecules. This assertion is further supported by the fact that the catalyst exhibiting favourable values of other properties (TTIP-isopropyl alcohol-1%Pt), like small particle size and high crystallinity (Table 6), did not display a high CH_4 production rate.

These results also clearly show that the addition of Pt to the TiO_2 catalyst markedly improves the photoactivity of the resulting catalyst in CH_4 production [44,60]. If the photocatalytic activities of Pt/TiO_2 are compared with those of TiO_2 photocatalysts obtained from the same Ti precursors and hydrolysis agents under the same synthesis conditions in supercritical CO_2 [45], we can see that there is an increase in CH_4/CO ratio for the Pt/TiO_2 catalysts (0.84–4.22) compared with those of their counterparts lacking Pt (0.03–0.30) (Table 7).

The CO production rate of the synthesised catalysts was about 90% lower than that of the commercial catalyst, even that of the synthesized catalyst with the highest CO formation rate (DIPBAT-ethanol-1%Pt). This observation cannot be explained only by the increase in the production of CH_4. The photochemical H_2O-gas shift reaction to produce H_2 and CO_2 from CO and H_2O may have occurred, lowering the yield of CO [60]. This reaction is often observed in the presence of noble metal/TiO_2 catalysts [60,63]. However, this does not seem a satisfactory explanation in these experiments given the low H_2O vapour/CO_2 ratio used [36]. Regarding the reaction time, Table 5 reveals that extending the photocatalytic reaction from 3 to 4 h did not substantially increase the CH_4 production rate. According to Habisreutinger et al. [49], this saturation of the product formation curve may be caused by strong adsorption of the O_2 produced in CO_2 photolysis, which may block reaction sites.

Table 8 compares CH_4 and CO production rates reported in recent studies for photocatalytic reduction of CO_2 with H_2O vapour as the reducing agent. The values are scarcely comparable because of the many variables are involved in the CO_2 reduction process. Generally, the CH_4 production rates obtained in this work are of the order of those reported for metal dispersed on TiO_2 particles, TiO_2 in the absence of metal, TiO_2 nanotubes and even metal/TiO_2 over optical fibres.

Nevertheless, we are aware that there is still room for improvement. On the one hand, some investigators have reported higher CH_4 production rates [7,8,11,13,14,70]; on the other

Table 7
Comparison of the photocatalytic activities of synthesised catalysts with and without Pt.

Catalyst	Pt loading (wt%)	Catalyst weight (mg)	H_2O/CO_2 (mol/mol)	Reaction time (h)	CH_4 /CO (mol/mol)
P-25	0	35.5	2/7	3	0.04
TTIP-isopropyl alcohol	1	34.6	2/7	3	1.24
TTIP-ethanol	1	39.6	2/7	3	4.22
DIPBAT-isopropyl alcohol	1	35.7	2/7	3	1.24
DIPBAT-ethanol	1	39.3	2/7	3	0.84
TTIP-isopropyl alcohol	0	41.3	2/7	3	0.03
TTIP-ethanol	0	31.9	2/7	3	0.16
DIPBAT-isopropyl alcohol	0	28.9	2/7	3	0.30
DIPBAT-ethanol	0	42.0	2/7	3	0.26

Table 8
Summary of reported CH_4 and CO production rates.

Catalyst	Metal	Reagent	Light source	Production rates (μmol g^{-1} h^{-1}) CH_4 (CO)	Ref.
TiO_2 anchored on Vycor glass	–	CO_2 H_2O	75 W Hg lamp	0.11	[64]
Quartz wool immersed in P-25 suspension	–	CO_2 H_2O	UV lamp	0.1 (< 0.1)	[65]
TiO_2 pellets	–	CO_2 H_2O	3 germicidal UVC lamps (4.8 W), 24 h	0.22 (< 0.16)	[66]
TiO_2 on glass beads	0.25 wt% Pt	CO_2 H_2O	75 W daylight lamp	0.3	[67]
P-25	–	CO_2 H_2O	100 W high pressure Hg lamp	0.2	[55]
TiO_2-SiO_2-acac/optical fiber	0.5 wt% Cu-0.5 wt% Fe	CO_2 H_2O	Sunlight	0.279	[68]
Titania nanotubes	–	CO_2 H_2O	100 W high pressure Hg lamp	0.3	[69]

hand, actual conversion efficiencies reported here and in previous studies are still quite low and should be increased by orders of magnitude before the CO_2 photoreduction process can be used in practical applications. Because of this, we are currently attempting to further enhance the photocatalytic activity of the TiO_2-based materials reported in this work.

Specifically, to increase the selectivity of the catalysts for the productions of CH_4 and methanol, three strategies are being followed: The use of TiO_2-based catalysts with enhanced geometries: TiO_2 nanofibres and TiO_2 nanotubes with and without metal modification [7,13]. The addition of non-metal elements to TiO_2 [8]. The synthesis of composite photocatalysts combining TiO_2 and reduced graphene oxide [9,10].

4. Conclusions

Photocatalysts with similar or better features, like high surface area, large pore volume, high crystallisation degree and high OH concentration, than those of commercial TiO_2 can be obtained by supercritical media synthesis. This method is more environmentally friendly and scalable than traditional techniques used to fabricate TiO_2-based photocatalysts. In addition, it is possible to improve the performance of catalysts by shifting their absorption spectra to the visible region if they are loaded with Pt at concentrations between 1 and 3 wt.%.

When the synthesised catalysts were used in CO_2 photoreduction in the gas phase, we detected CH_4 and CO as the main products at the end of the reaction time, which is in agreement with one of the possible reduction mechanisms described in the literature. The CH_4 production rates of the catalysts synthesised in this work were clearly improved compared with that of a commercial catalyst and better or similar to those reported in the literature for catalysts synthesised with more expensive and laborious procedures.

To sum up, photochemical conversion of CO_2 constitutes not only an innovative technique to reduce greenhouse gas emission, but also a potential alternative to the depletion of fossil fuel resources. Although it is clear that the catalysts synthesised to date for CO_2 reduction to fuel cannot yet be commercially applied, we expect that further developments will allow them to be in the near future. To achieve this goal, further work on photocatalyst design must combine the improvement in solar light response with the control of the efficiency and selectivity of the CO_2 photoreduction process.

References

[1] Intergovernmental Panel on Climate Change (IPCC), Working Group I Contribution to the IPCC Fifth Assessment Report Climate Change 2013: The Physical Science Basis. Technical Summary, **2013** (http://www.climatechange2013.org/images/report/WG1AR5_ALL_FINAL.pdf).
[2] S. Chakravarti, A. Gupta, U.S. Patent 6 165 433, **2000**.
[3] O. Zelayandia, WO Patent WO2007022595 A1, **2007**.
[4] O. K. Varghese, M. Paulose, T. J. LaTempa, C. A. Grimes, *Nano Lett.*, **2009**, 9, 731–737.
[5] S. C. Roy, O. K. Varghese, M. Paulose, C. A. Grimes, *ACS Nano*, **2010**,

Graphical Abstract

Chin. J. Catal., 2017, 38: 636–650 doi: 10.1016/S1872-2067(17)62766-9

Supercritical synthesis of platinum-modified titanium dioxide for solar fuel production from carbon dioxide

Susana Tostón, Rafael Camarillo*, Fabiola Martínez, Carlos Jiménez, Jesusa Rincón
University of Castilla-La Mancha, Spain

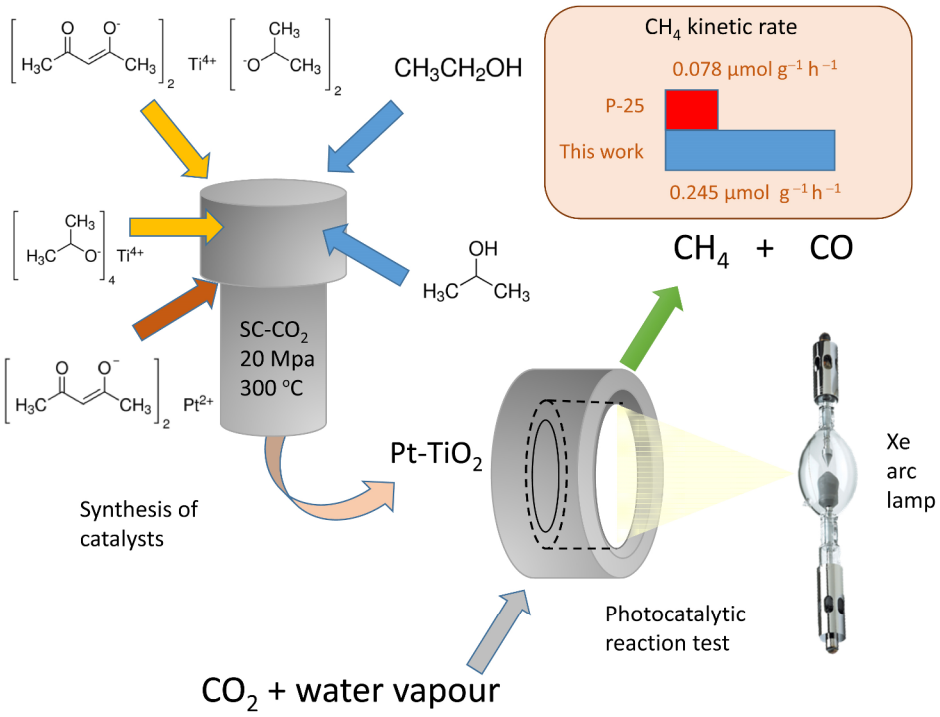

The catalytic properties of Pt/TiO_2 particles can be tuned by simply changing operating parameters like the type of titania precursor and/or hydrolysis agent when their hydrothermal formation reaction is accomplished in supercritical CO_2. The synthesised particles exhibit superior performance to that of a commercial catalyst in the photocatalytic reduction of CO_2 to methane.

4, 1259–1278.
[6] S. Neatu, J. A. Maciá-Agulló, H. Garcia, *Int. J. Mol. Sci.*, **2014**, 15, 5246–5262.
[7] Y. F. Li, W. P. Zhang, X. Shen, P. F. Peng, L. B. Xiong, Y. Yu, *Chin. J. Catal.*, **2015**, 36, 2229–2236.
[8] M. S. Akple, J. X. Low, Z. Y. Qin, S. Wageh, A. A. Al-Ghamdi, J. G. Yu, S. Liu, *Chin. J. Catal.*, **2015**, 36, 2127–2134.
[9] L. C. Sim, K. H. Leong, P. Saravanan, S. Ibrahim, *Appl. Surf. Sci.*, **2015**, 358, 122–129.
[10] J. X. Low, B. Cheng, J. G. Yu, *Appl. Surf. Sci.*, **2017**, 392, 658–686.
[11] Z. Q. He, J. T. Tang, J. Shen, J. M. Chen, S. Song, *Appl. Surf. Sci.*, **2016**, 364, 416–427.
[12] M. Tahir, B. Tahir, N. A. S. Amin, *Appl. Surf. Sci.*, **2015**, 356, 1289–1299.
[13] P. Reñones. A. Moya, F. Fresno, L. Collado, J. J. Vilatela, V. A. de la Peña O'Shea, *J. CO_2 Util.*, **2016**, 15, 24–31.
[14] J. Y. Do, V. Tamilavan, R. Agneeswari, M. H. Hyun, M. Kang, *J. Photochem. Photobio. A*, **2016**, 330, 30–36.
[15] A. Zaleska, *Recent Pat. Eng.*, **2008**, 2,157–164.
[16] C. Ampelli, R. Passalacqua, C. Genovese, S. Perathoner, G. Centi, T. Montini, V. Gombac, J. J. Delgado Jaen, P. Fornasiero, *RSC Adv.*, **2013**, 3, 21776–21778.
[17] C. Ampelli, C. Genovese, R. Passalacqua, S. Perathoner, G. Centi, *Appl. Therm. Eng.*, **2014**, 70, 1270–1275.
[18] M. A. Henderson, *Surf. Sci. Rep.*, **2011**, 66, 185–297.
[19] Y. Ma, X. L. Wang, Y. S. Jia, X. B. Chen, H. X. Han, C. Li, *Chem. Rev.*, **2014**, 114, 9987–10043.
[20] Q. H. Zhang, W. D. Han, Y. J. Hong, J. G. Yu, *Catal. Today*, **2009**, 148, 335–340.
[21] G. N. Kryukova, G. A. Zenkovets, A. A. Shutilov, M. Wilde, K. Günther, D. Fassler, K. Richter, *Appl. Catal. B*, **2007**, 71, 169–176.
[22] F. Chekin, S. Bagherib, S. B. Abd Hamidb, *Sensors Actuat. B*, **2013**, 177, 898–903.
[23] S. Semlali, T. Pigot, D. Flahaut, J. Allouche, S. Lacombe, L. Nicole, *Appl. Catal. B*, **2014**, 150–151, 656–662.
[24] Y. Hu, X. Song, S. M. Jiang, C. H. Wei, *Chem. Eng. J.*, **2015**, 274, 102–112.
[25] A. Ofiarska, A. Pieczyńska, A. Fiszka Borzyszkowska, P. Stepnowski, E. M. Siedlecka, *Chem. Eng. J.*, **2016**, 285, 417–427.
[26] Z. Xiong, H. B. Wang, N. Y. Xu, H. L. Li, B. Z. Fang, Y. C. Zhao, J. Y. Zhang, C. G. Zheng, *Int. J. Hydrogen Energy*, **2015**, 40, 10049–10062.
[27] R. Pol, M. Guerrero, E. García-Lecina, A. Altube, E. Rossinyol, S. Garroni, M. D. Baró, J. Pons, J. Sort, E. Pellicer, *Appl. Catal. B*, **2016**, 181, 270–278.
[28] H. Fernández-Rodríguez, E. Alonso, M. J. Cocero, Síntesis en medio supercrítico de materiales para su utilización en reacciones catalíticas heterogéneas, Book of abstracts Flucomp, Madrid, **2009**.
[29] A. de Lucas, J. Rincón, I. Gracia, *J. Am. Oil Chem. Soc.*, **2003**, 80,

181–188.
[30] J. Rincón, R. Camarillo, L. Rodríguez, V. Ancillo, *Ind. Eng. Chem. Res.*, **2010**, 49, 2410–2418.
[31] J. Rincón, A. De Lucas, I. Gracia, *Sep. Sci. Technol.*, **2000**, 35, 2745–2763.
[32] J. Rincón, F. Martínez, L. Rodríguez, V. Ancillo, *J. Supercrit. Fluids*, **2011**, 56, 72–79.
[33] E. Alonso, I. Montequi, S. Lucas, M. J. Cocero, *J. Supercrit. Fluids*, **2007**, 39, 453–461.
[34] S. Tostón, R. Camarillo, F. Martínez, C. Jiménez, J. Rincón, *Res. J. Chem. Environ.*, **2014**, 18, 46–53.
[35] D. Uner, M. M. Oymak, *Catal. Today*, **2012**, 181, 82–88.
[36] C. J. Wang, R. L. Thomson, J. Baltrus, C. Matranga, *J. Phys. Chem. Lett.*, **2010**, 1, 48–53.
[37] N. Aman, P. K. Satapathy, T. Mishra, M. Mahato, N. N. Das, *Mater. Res. Bull.*, **2012**, 47, 179–183.
[38] E. Alonso, I. Montequi, M. J. Cocero, *J. Supercrit. Fluid.*, **2009**, 49, 233–238.
[39] G. Wu, T. Nishikawa, B. Ohtani, A. Chen, *Chem. Mater.*, **2007**, 19, 4530–4537.
[40] Y. Shih, C. Lin, *Environ. Sci. Pollut. Res.*, **2012**, 19, 1652–1658.
[41] N. Balazs, K. Mogyorosi, D. F. Sranko, A. Pallagi, T. Alapi, A. Oszko, A. Dombi, P. Sipos, *Appl. Catal. B*, **2008**, 84, 356–362.
[42] J. G. Yu, W. G. Wang, B. Cheng, B. L. Su, *J. Phys. Chem. C*, **2009**, 113, 6743–6750.
[43] Q. Wang, D. Yang, D. M. Chen, Y. B. Wang, Z. Y. Jiang, *J. Nanopart. Res.*, **2007**, 9, 1087–1096.
[44] J. Mao, L. Q. Ye, K. Li, X. H. Zhang, J. Y. Liu, T. Y. Peng, L. Zan, *Appl. Catal. B*, **2014**, 144, 855–862.
[45] R. Camarillo, S. Tostón, F. Martínez, C. Jiménez, I. Asencio, J. Rincón, *J. Earth Sci. Clim. Change*, **2016**, 7(9), 149.
[46] R. Camarillo, J. Rincón, *Chem. Eng. Technol.*, **2011**, 34, 1675–1684.
[47] B. K. Avasarala, S. R. Tirukkovalluri, S. Bojja, *Int. J. Mater. Res.*, **2010**, 101, 1563–1571.
[48] A. L. Patterson, *Phys. Rev.*, **1939**, 56, 978–982.
[49] S. N. Habisreutinger, L. Schmidt-Mende, J. K. Stolarczyk, *Angew. Chem. Int. Ed.*, **2013**, 52, 7372–7408.
[50] E. Reverchon, G. Caputo, S. Correra, P. Cesti, *J. Supercritic. Fluids*, **2003**, 26, 253–561.
[51] I. Tanabe, Y. Ozaki, Y., *Chem. Commun.*, **2014**, 50, 2117–2119.
[52] F. Gracia, J. P. Holgado, A. Caballero, A. R. Gonzalez-Elipe, *J. Phys. Chem. B*, **2004**, 108, 17466–17476.
[53] A. L. Linsebigler, G. Q. Lu, J. T. Yates Jr., *Chem. Rev.*, **1995**, 95, 735–758.
[54] S. Bagwasi, B. Tian, F. Chen, J. Zhang, *Appl. Surf. Sci.*, **2012**, 258, 3927–3935.
[55] M. Kitano, M. Matsuoka, M. Ueshima, M. Anpo, *Appl. Catal. A*, **2007**, 325, 1–14.
[56] H. Zhang, X. J. Lv, Y. M. Li, Y. Wang, J. H. Li, *ACS Nano*, **2010**, 4, 380–386.
[57] Y. Zhang, P. Zhang, Y. N. Huo, D. Q. Zhang, G. S. Li, H. X. Li, *Appl. Catal. B*, **2012**, 115–116, 236–244.
[58] X. K. Li, Z. J. Zhang, W. Li, H. Q. Pan, *Appl. Catal. A*, **2012**, 429–430, 31–38.
[59] P. Usubharatana, D. McMartin, A. Veawab, P. Tontiwachwuthikul, *Ind. Eng. Chem. Res.*, **2006**, 45, 2558–2568.
[60] T. Yui, A. Kan, C. Saitoh, K. Koike, T. Isubuki, O. Ishitani, *ACS Appl. Mater. Interfaces*, **2011**, 3, 2594–2600.
[61] M. Anpo, H. Yamashita, Y. Ichihashi, S. Ehara, *J. Electroanal. Chem.*, **1995**, 396, 21–26.
[62] M. Marszewski, S. W. Cao, J. G. Yu, M. Jaroniec, *Mater. Horiz.*, **2015**, 2, 261–278.
[63] T. D. Nguyen-Phan, A. E. Barber, J. A. Rodríguez, S. D. Senanayake, *Appl. Catal. A*, **2016**, 518, 18–47.
[64] M. Anpo, K. Chiba, *J. Mol. Catal.*, **1992**, 74, 207–212.
[65] F. Saladin, L. Forss, I. Kamber, *J. Chem. Soc. Chem. Commun.*, **1995**, 533–534.
[66] S. Sing Tan, L. Zou, E. Hu, *Sci. Technol. Adv. Mater.*, **2007**, 8, 89–92.
[67] O. Ozcan, F. Yukruk, E. U. Akkaya, D. Uner, *Appl. Catal. B*, **2007**, 71, 291–297.
[68] T. V. Nguyen, J. C. S. Wu, *Appl. Catal. A*, **2008**, 335, 112–120.
[69] B. K. Vijayan, N. M. Dimitrijevic, J. Wu, K. A. Gray, *J. Phys. Chem. C*, **2010**, 114, 21262–12269.
[70] J. Pan, X. Wu, L. Z. Wang, G. Liu, G. Q. Lu, H. M. Cheng, *Chem. Commun.*, **2011**, 47, 8361–8363.